FACTA UNIVERSITATIS
Series: **Electronics and Energetics** Vol. 32, N° 4, December 2019, pp. 513-528
https://doi.org/10.2298/FUEE1904513M

DESIGNING METHOD FOR INTEGRATED BATTERY CHARGERS IN ELECTRICAL VEHICLES

Aleksandar Milic, Slobodan Vukosavic

University of Belgrade, Dept. of Electrical Engineering, Serbia

Abstract. *Electrical vehicles often make use of multi-phase induction motors. At the same time, the vehicles have an on-board charger, the power electronics device that converts the ac power from the mains and charges the traction battery. The traction inverter can be integrated with the charger, reducing in this way the component count, weight and cost, while the windings of the ac motor can be used as the inductors required to complete the charger topology, thus saving on passive components, iron and copper. The integrated charger performances depend on the configuration of the stator windings as well as on the topology of the power converter. The objective in charging mode is reaching a high efficiency while keeping the charging-mode electromagnetic torque at zero. In traction mode, the goals include the efficiency and the torque-per-Amps ratio. In order to compare and distinguish between the available topologies and configurations, the paper starts with the analysis of the magnetic field in the air-gap of the electric machine in both charging and traction modes. Based upon that, a novel algorithm is proposed which determines the space-time distribution of the air-gap field, eventually deriving all the relevant pulsating and revolving component of the magnetic field, thus providing the grounds for studying the losses, efficiency and torque pulsations in both charging and traction modes.*

Key words: *Induction machines, machines, battery chargers, electric vehicles*.

Nomenclature

Parameter	**Designator (Unit)**
Number of stator slots	$N_s = 36$
Grid currents	i_n [A]; phase number $n = 1,2\ldots6$
Stator currents	i_{mn} [A]; phase number n = 1,2…9
Angular frequency	ω [rad/s]
Stationary-frame currents	i_α, i_β [A]
Additional current components	$i_x, i_y, i_{x1}, i_{y1}, i_{x2}, i_{y2}$ [A]
Current amplitude per slot	$I = 1\ A$
Phase shift	φ [rad]
Frequency	$f = 50$ Hz
Time-discretization	$\Delta t = 1\ ms$
Harmonic order	$v = 1, 3, 5\ldots 19$
MMF harmonic components	F_{vs} [A]
Spatial displacement of the individual phase magnetic axis	δ [rad]

Received January 8, 2019; received in revised form March 12, 2019
Corresponding author: Aleksandar Milic
University of Belgrade, Dept. of Electrical Engineering, 11000 Belgrade, Serbia
(E-mail: milic.aleksandar@etf.rs)

1. INTRODUCTION

The use of vehicles with internal combustion engines (ICM) in urban areas has adverse effects on the local environment, and it also contribute to emission of pollutants and greenhouse gasses. Although the first electric vehicles (EV) were introduced in 19. century, their use subsided after the introduction of low-cost Model T - Ford. In an attempt to reduce and control emissions and their harmful effects on humans and the environment, electrical vehicles are regaining attention.

In rural and open areas, the internal combustion engines [1] with spark-plug-controlled compression-ignition gasoline engines could acquire the potential of developing a new solution, more acceptable for the environment than the electrical vehicles that run on electrical energy obtained from the power utilities. There are opinions [2] that the green house gas emissions from power utilities in conjunction with emissions from the factories that manufacture EV, their batteries and other key parts could match, and, in some cases, even exceed the emissions of ICM vehicles. This opinion is opposite to many other reports. In urban, densely populated areas, a vast number of ICM vehicles concentrates emissions and pollutes the air. Therefore, there are all the good reasons to substitute ICM-driven vehicles by EV in all urban areas and other places where local environmental conditions are of particular importance. In general, the electrification of transportation has the potential of reducing the use of fossil fuels, but the green-house gasses emissions largely depend on the primary source mix for the electricity generation [3].

The vehicles that run on electricity require the equipment for the battery charging. In order to improve efficiency, regenerate the kinetic energy and enable the use in urban areas, most modern ICM-vehicles are hybrid, and they also include an electrical machine, power electronics devices and the means for the energy accumulation. This emphasizes the significance of designing light-weight, low-cost integrated battery chargers and optimizing their configuration and topology so as to maximize the performances in both charging and traction mode.

Conventional chargers comprise their switching stages and passive L and C components separate from the traction motor and the traction converter. Their weight and size adds to the weight and size of the traction converter and the traction motor. Since the traction and charging do not take place at the same time, devices used in traction mode can be used for charging and vice versa. In integrated chargers, the passive filtering components of the charger are replaced by the stator winding, while the traction converter can be put to use as the switched-mode controller of the charging currents. In the prescribed manner, the overall weight and size of passives and switching devices is considerably reduced, making the integrated chargers preferred choice [4]-[8].

The chargers could be installed on-board the EV, which simplifies the stationary part of the charging system. Off-board systems provide fast charging, an ease of installation and galvanic isolation [4], but their connections have electrical and mechanical features that are closely related to the EV and its battery. On the other hand, on-board systems require just an ac socket and the cable connection to the mains, paving the way to a more general and widespread use [5] in all the cases where the cable connection is acceptable. Thus, it is of interest to study integrated-charger topologies which reduce the weight, space and cost of the on-board equipment [6]-[8].

While in charging mode, it is necessary to maintain sinusoidal line-current waveforms and unity power factor in order to maximize the power for the rated current [9]. In topology

shown in Fig. 1, the stator phase windings of the traction motor are connected to a three-phase grid and used as input line filter of the integrated charger. Both the inverter and the dc/dc converter are bidirectional. As the charging and traction modes do not take place simultaneously, the equipment shown in Fig. 1 serves both purposes. While the system is in charging mode, the charging currents can create the revolving magnetic field and electromagnetic torque that could stir the rotor into motion. Any motion and consequential electromotive forces are undesired and harmful, as they interfere with the charging process, increase the losses and jeopardize safety. The problem of the rotor movements can be solved by adopting mechanical brakes or using an appropriate clutch [10], [11]. Both approaches require additional mechanical parts that require maintenance and increase weight and size of the motor. Even in cases where the rotor is blocked by mechanical brakes, revolving magnetic fields caused by the charging currents would create additional losses and reduce the efficiency. In cases where the braking is accomplished by electrical means [12], it comes at the cost of increased losses within the motor.

While in some cases the revolving fields do not exist in charging mode, others may require additional power switches and/or re-configuration of the windings while in charging mode [13]-[15]. Advantage of multiphase machines is the possibility to obtain zero-revolving-fields conditions during the charging with no additional switches and without the reconnection of the windings.

The operation of integrated chargers with multiphase machines depend on the power converter topology and also on the configuration of the stator winding and the magnetic circuit. The impact of design parameters and choices on the system performances has to be studied in order to distinguish the optimum converter-machine match, the one that meets the requirements in both charging and traction modes. Commonly used design methods rely on Finite-Element models and tools [16]. In most cases, design and optimization of electrical machines [17], [18] includes iteration and/or search procedures. Whether driven by meta-heuristic or similar algorithms, most procedures include considerable number of successive design attempts. An intent to use the FEM tools in each attempt is impractical, and there is a need to devise a simple and quick approach to computing the key performances from the attempted design parameters and choices.

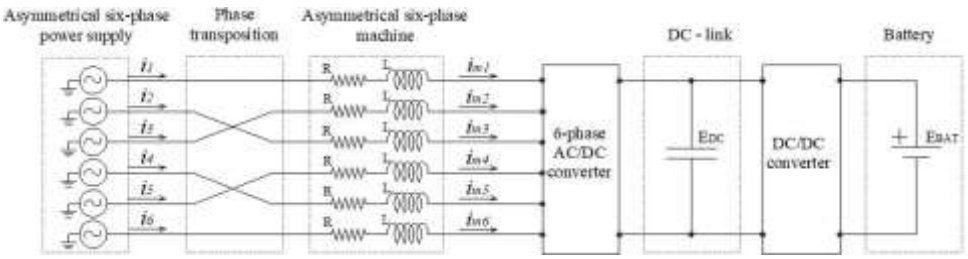

Fig. 1 Integrated charger with battery dc/dc converter, 6-phase inverter and 6-phase asymmetrical machine. Notice that the 6-phase power supply requires a set of conveniently arranged transformers.

In this paper, a novel approach to deriving the key performances of machine-converter system is derived. Proposed approach is considerably faster as it avoids

laborious finite-element analysis. Design is expressed in terms of the stator-winding parameters, parameters of the magnetic circuit and the main features of the power converter. The input data is used to derive the principal pulsating and revolving air-gap fields, which are used thereafter to compare the losses and pulsating torques of attempted machine-converter designs. The core of the proposed approach is the algorithm which evaluates the impact of the winding configuration and the converter topology on the space-time distribution of the air-gap magnetic field in integrated chargers. Analytical approach to obtaining the air-gap field distribution is given in Section II. A novel algorithm that distinguishes the relevant pulsating and revolving fields is developed in Section III. In Section IV, proposed solution is verified by performing simulations of several cases with 6- and 9-phase machines in both traction and charging modes. Conclusions are given in Section V. All variables are given in nomenclature.

2. ANALYTICAL CONSIDERATIONS

In Fig. 2, an integrated charger connects to the 3-phase grid. With multiphase machines with $3q$ phases, each phase of the mains connects to q phases of the stator winding. The stator winding configuration determines the topology of the static power converter that is used both for the charging mode and for the traction mode. Whenever possible, the configuration is supposed to be conceived to zero-out the revolving fields in the case of the battery charging.

Specific transformation matrix for the phase currents is required for each configuration of the stator winding [19]. Transformation matrix of [19] provides the usual torque-producing currents i_d and i_q, but also additional current components which do not produce the torque. Such additional components do not exist in the case of a conventional 3-phase machine. The pairs of current components such as (i_d, i_q) and (i_x, i_y) can be represented as complex numbers, also called the space vectors that could be represented in two-dimensional plane. The currents that do not contribute to the torque represent a degree of freedom that could be used to optimize other design criteria, such as the operation of the system in charging mode. The transformation matrix of [19] is applied to a 5-phase machine, thus resulting in *d*, *q*, *x*, and *y* components that could be represented by vectors in two different planes, *d*-*q* and *x*-*y*. With the former being the key parts in torque generations, the later provide the degree of freedom required in suiting the proper torque-free battery charging process.

The example given in Fig. 1 presents an asymmetric six-phase machine used within an integrated charger. Magnetic axes of individual phases are spatially shifted by 30º. Even and odd phases can be grouped in two triplets. By the proper connection, these triplets can be connected in two distinct stars-of-windings. In order to develop the electromagnetic torque and achieve the normal traction functionality, it is necessary to supply the stator winding by the set of currents given in (1), where the phase shifts φ_1-φ_6 have to be adjusted so as to provide the revolving air-gap field of a constant amplitude.

$$i_{1,2,3,4,5,6} = I \sin(\omega t - \varphi_{1,2,3,4,5,6}) \tag{1}$$

The phase transposition illustrated in Fig. 1 is given in (2). Employing the decoupling transformation matrix for an asymmetrical six-phase machine from [21], the results are obtain that are given in (3).

$$i_{m2} = i_3, i_{m3} = i_2, i_{m4} = i_5, i_{m5} = i_4 \tag{2}$$

$$i_x = \sqrt{6}I\cos(\omega t),\ \ i_y = \sqrt{6}I\sin(\omega t),\ \ \ i_\alpha = 0,\ \ \ i_\beta = 0 \tag{3}$$

With the stationary-frame current components α-β equal to zero, the system in given conditions does not develop any revolving magnetic field. Thus, the charging replies on *x*-*y* current components, having the angular frequency ω and the amplitude sqrt(6)**I*. In a very like way, the system illustrated in Fig. 2 can be analyzed and explained. This system comprises a nine-phase machine where the machine phases are conveniently grouped in three stars. While in the charging mode, each star connection is attached to one of the three input phases. Rather than the setup of Fig. 1, the setup of Fig. 2 can be connected to the mains without any additional transformers. According to the analysis of [22], the mains currents i_1, i_2 and i_3 (Fig. 2) are given in (4), while the winding currents while charging are given in (5).

$$i_1 = I\sin(\omega t),\ i_2 = I\sin(\omega t - \frac{2\pi}{3}),\ i_3 = I\sin(\omega t - \frac{4\pi}{3}) \tag{4}$$

$$i_{m1,2,3} = i_1/3,\ i_{m4,5,6} = i_2/3,\ i_{m7,8,9} = i_3/3 \tag{5}$$

$$\begin{aligned} &i_\alpha = 0,\ i_\beta = 0,\ i_{x1} = I\left[2/3\cos(\omega t) + \sqrt{3}/3\sin(\omega t)\right], \\ &i_{y1} = -I\sqrt{3}/3\cos(\omega t),\ i_{x2} = i_{y2} = i_{x3} = i_{y3} = 0 \end{aligned} \tag{6}$$

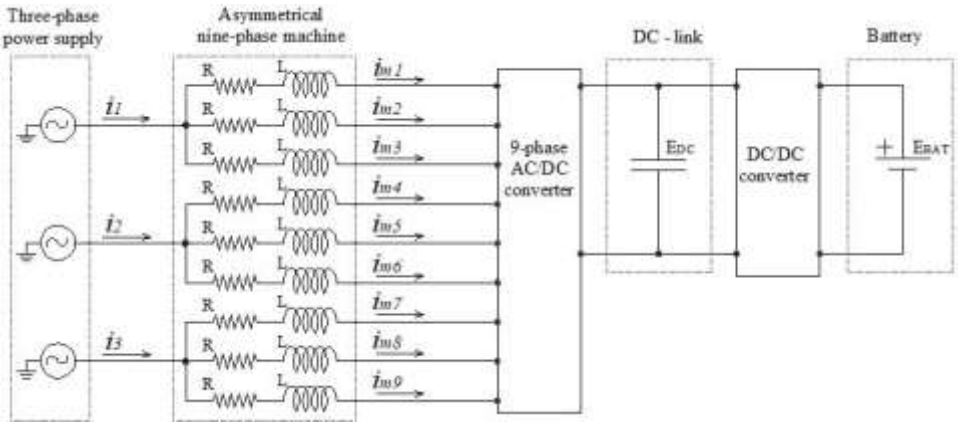

Fig. 2 Connections of the integrated charger with asymmetrical 9-phase machine

According to [22], the currents of (5) can be transformed and decomposed in α–β and *x*-*y* pairs given in (6). With α–β components, the revolving field in the air-gap is equal to zero, while the currents x_1-y_1 are responsible for the charging. The nine-phase topology of Fig. 2 connects to the mains without any additional components and with no re-wiring of the circuit. Getting the integrated charger with asymmetric 6-phase machine [21] in charging mode is more involved, but, on the other hand, the 6-phase topology has the advantage of having a smaller component count.

3. ANALYSIS OF THE AIR-GAP FIELD

The analysis given in this Section derives space harmonics of the air-gap field for integrated chargers given in Figs. 1 and 2. The former uses a six-phase source derived from the mains by means of a dedicated transformer [21], while the later connects the mains to the three star connections of the nine-phase winding [22]. The objective of the analysis is to consider the charging process and derive any and all the revolving and pulsating air-gap fields. It is of interest to derive the approach which distinguishes the field components for all the relevant stator-winding-configurations and all the relevant topologies of the power converter. The ultimate goal is to improve the design in order to maximize the performances of the system in both charging and traction modes.

Extraction of the pulsating and revolving fields cannot be perform by means of the conventional tools, such as the Fourier transformation. On the other hand, the problem complexity includes a non-sinusoidal winding and magnetomotive-force functions, which contribute to a great deal of space-time components of the air-gap field, including rather high orders. An accurate distribution of the air-gap field can be obtained by FEM tools, but this approach is laborious and incompatible with the needs, as it requires considerable time and effort, and it can hardly be used in iterative loops. Therefore, the approach outlined hereafter adopts the following reasonable assumptions: (1) The main part of the *magnetic-voltage-drop* is experienced in the air-gap, and (2) While the air-gap circumference can be divided in N_s parts, N_s being the number of the stator slots, the magnetomotive-force (MMF) can be obtained by integrating the field strength under each stator tooth, thus neglecting the non-homogeneous field distribution caused by the specific form of the slots and teeth of the magnetic circuit. In addition to these, it is also assumed that magnetic saturation is not emphasized. The later assumption on linearity simplifies the subsequent calculations: it is sufficient to calculate the MMF for only one amplitude of the sinusoidal stator currents, assuming that the MMF values for other amplitudes would change proportionally. In further considerations, the current amplitude is scaled down to 1A per slot. To obtain further time savings, it is assumed that 50Hz waveforms can be represented by time-discretization of 1 ms.

Proposed procedure envisages the following steps: (i) Given the winding configuration and converter topology, the time-space samples of the corresponding MMF are calculated at specific instants for each of the discrete locations along the circumference; (ii) An analytical function is devised comprising the reasonable number of low-order harmonics, suited to fit the MMF as the function of time and space, said function comprising the set of parameters (amplitudes and shifts) yet to be determined; (iii) The time-space samples of the MMF obtained in first step are used to calculate the parameters of the function devised in the second step. In order to obtain the best-fit in terms of the sum of the square of residues (errors), the adopted approach includes Moore-Penrose inversion of rectangular matrix [23], [24] wherein the number of matrix rows (equations) exceeds the number of columns (parameters) by several orders of magnitude; (iv) Finally, all the revolving and pulsating magnetic fields are obtained from the function devised in the second step an provided with the parameters obtained in the third step.

The waveforms given in Figs. 3 and 4 correspond to the MMF obtained with the two sample designs. The waveforms are given for t=5ms, t=10ms, t=15ms, and t=20ms, with the angle (space) given on horizontal axes. At this point, it is necessary to attempt the corresponding analytical expressions. Without the lack of generality, it can be assumed

that the instant that corresponds to $\theta = 0$ is such that the target function is an odd function, and that the order of relevant harmonics ends with $v = 19$. In this case, the MMF distribution obtained from one phase is given in (7), where the amplitudes F_{1S}, F_{3S}, …, F_{19S} have yet to be defined.

$$f(\theta) = F_{1s}\sin\theta - F_{3s}\sin 3\theta + F_{5s}\sin 5\theta - F_{7s}\sin 7\theta + ... - F_{19s}\sin 19\theta \tag{7}$$

While (7) represents the distribution of the MMF along the circumference for one of the phases, other phases have similar formula. Yet, due to the spatial shifts between magnetic axes of individual phases, other phases may require the functions $f(\theta)$ which include both sine and cosine components with corresponding amplitudes. Denoting the spatial displacement of the magnetic axis of individual phase by δ and the phase shift by φ, the corresponding MMF expression is given in (8). The expression is derived assuming that all the phase currents have the same amplitude I.

$$\begin{aligned} f(\theta,t) = I\sin(\omega t - \varphi)\big[&F_{1s}\sin(\theta-\delta) + F_{1c}\cos(\theta-\delta) - F_{3s}\sin 3(\theta-\delta) - \\ &-F_{3c}\cos 3(\theta-\delta) + ... - F_{19s}\sin 19(\theta-\delta) - F_{19c}\cos 19(\theta-\delta)\big] \end{aligned} \tag{8}$$

The obtained results can be used to derive analytical expression that describes space-time distribution of the magnetomotive force for the integrated charger with 6-phase machine, shown in Fig. 1. Corresponding expression derived for the charging mode is given in (9). Due to specific configuration of the stator windings and the spatial displacement of magnetic axes, the expression does not comprise any even nor the harmonics with of order that is a multiple of three. Due to the phase transposition, the considered six-phase asymmetrical stator winding does not generate harmonics of the 11th and 13th order, nor does it produce any fundamental component.

$$\begin{aligned} f_{6asy}^{eq}(t,\theta) = {} & \mathrm{F}_{c5}\sin(\omega\mathrm{t}\text{-}5\theta) + \mathrm{F}_{s5}\cos(\omega\mathrm{t}\text{-}5\theta) \\ & \text{-}\mathrm{F}_{c7}\sin(\omega\mathrm{t}\text{+}7\theta) + \mathrm{F}_{s7}\cos(\omega\mathrm{t}\text{+}7\theta) \\ & +\mathrm{F}_{c17}\sin(\omega\mathrm{t}\text{-}17\theta) + \mathrm{F}_{s17}\cos(\omega\mathrm{t}\text{-}17\theta) \\ & \text{-}\mathrm{F}_{c19}\sin(\omega\mathrm{t}\text{+}19\theta) + \mathrm{F}_{s19}\cos(\omega\mathrm{t}\text{+}19\theta) \end{aligned} \tag{9}$$

When the 9-phase machine of Fig. 2 is used in charging mode, each of the 3-phase mains voltages is fed into the star connection of one of the three groups that comprise three phase winding each. The three stars with three phase windings each create the stator winding system of 9-phase machine. The charging current in said windings creates pulsating magnetic field [5]. The resultant MMF which comprises the contribution of all the phases in charging mode is given in (10), and it has a strictly pulsating nature. From (10), the only harmonics of the pulsating field are of order 3, 9 and 15, while the harmonics of the order 1, 5, 7, 11, 13, 15 and 19 are absent.

$$
\begin{aligned}
f_{9asy}^{eq}(t,\theta) = & -F_{3c}[\sin(\omega t-3\theta)+\sin(\omega t+3\theta)] \\
& -F_{3c}[\sin(\omega t-3\theta-2\pi/3)+\sin(\omega t-3\theta-\pi/3)] \\
& -F_{3s}[\cos(\omega t-3\theta)-\cos(\omega t+3\theta)] \\
& -F_{3s}[\cos(\omega t-3\theta-2\pi/3)+\cos(\omega t-3\theta-\pi/3)] \\
& +F_{9c}[\sin(\omega t-9\theta)+\sin(\omega t+9\theta)] \\
& +F_{9s}[\cos(\omega t-9\theta)-\cos(\omega t+9\theta)] \\
& +F_{9c}[\sin(\omega t-9\theta+\pi/3)+\sin(\omega t+9\theta+\pi/3)] \\
& +F_{9s}[\cos(\omega t-9\theta+\pi/3)-\cos(\omega t+9\theta+\pi/3)] \\
& +F_{9c}[\sin(\omega t-9\theta+2\pi/3)+\sin(\omega t+9\theta+2\pi/3)] \\
& +F_{9s}[\cos(\omega t-9\theta+2\pi/3)-\cos(\omega t+9\theta+2\pi/3)] \\
& -F_{15c}[\sin(\omega t-15\theta)+\sin(\omega t+15\theta)] \\
& -F_{15c}[\sin(\omega t+15\theta-2\pi/3)+\sin(\omega t+15\theta-\pi/3)] \\
& -F_{15s}[\cos(\omega t-15\theta)-\cos(\omega t+15\theta)] \\
& -F_{15s}[-\cos(\omega t+15\theta-2\pi/3)-\cos(\omega t+15\theta-\pi/3)]
\end{aligned}
\tag{10}
$$

Analytical expressions that are obtained for the cases illustrated in Figs. 1 and 2 are used in the subsequent considerations. For each of the considered systems, the functional approximation can take into account the space-time distribution of the field in both the traction mode, when the electrical machine operates with prevalently revolving magnetic fields and generates the moving torque, and in charging mode, where the revolving fields are not desired, while the amplitude of the remaining pulsating fields has to be reduced in order to curb down the losses. In deriving the functional approximation and parameter-fitting of the relevant functions, proposed procedure describes pulsating fields as the sum of the two revolving fields having the same speed and amplitude but different directions (11). In addition to pulsating fields, the air-gap field comprises a set of revolving fields that run at different speeds in direct or inverse sense. All the fields components produce the losses, but only the revolving fields are responsible for the torque generation.

$$
f_{\nu}(t,\theta) = F_{\nu}[\sin(\omega t-\nu\theta)+\sin(\omega t+\nu\theta)] \tag{11}
$$

Analytical representations of the magnetomotive force in (9) and (10) depict the air-gap field dependence on space (that is, position along the circumference) and time. Expression (9) and Fig. 3 correspond to the six-phase asymmetrical machine. Expression (10) and Fig. 4 correspond to the nine-phase machine. The field in Fig. 4 and (10) comprises several revolving and several pulsating components. It is also observed that the revolving-field content is considerably lower in nine-phase machine.

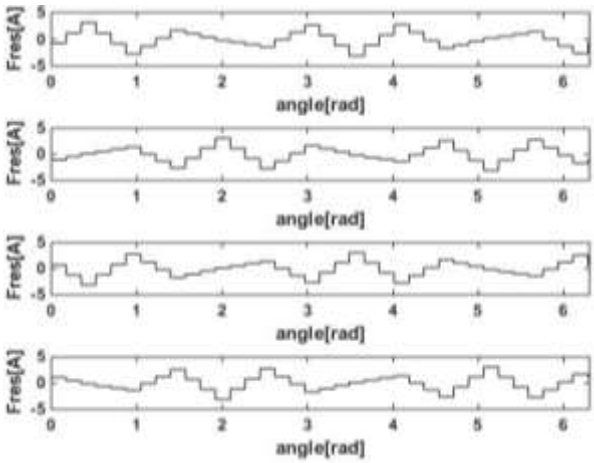

Fig. 3 Spatial distribution of the air-gap field in an asymmetrical six-phase machine used within the integrated charger of Fig. 1. The waveforms are taken at 4 distinct instants of time.

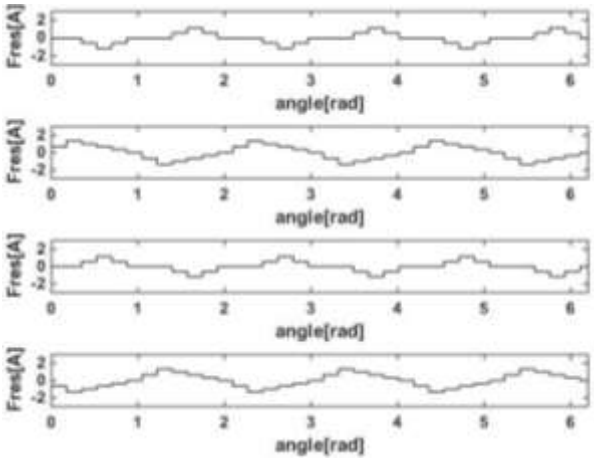

Fig. 4 Spatial distribution of the air-gap field in an asymmetrical nine-phase machine used within the integrated charger of Fig. 2. The waveforms are captured at 4 distinct instants of time.

The next step of the proposed procedure consists in deriving the coefficients that correspond to the amplitudes of the specific fields components in (9) and (10). The relevant input data points for such procedure are the time-samples of the MMF taken within one period of the excitation current (that is, one period of the mains) for each of the preselected discrete locations along the circumference. Based on the previous considerations, the time-samples are taken each 1ms within the period of 20ms. In a machine with 36 slots, there are 36 locations where the MMF is calculated. In the prescribed way, there is a total of 720 equations that express the MMF values at specific

time and space instants. In addition to the specific time (t_x), space (θ_x) and readily available $MMF = f(t_x,\theta_x)$ obtained in the previous step, each of 720 equations also comprises the desired parameters, that is, the coefficients that correspond to the amplitudes of the specific fields components in (9) and (10).

Based on the previous considerations, the functional approximation of the air-gap field in an 6-phase machine requires 8 coefficients. The number of equations (720) exceeds the number of unknown parameters by far. Therefore, it is not possible to find the parameter set that would bring all the equations in the balance, as any and all of them may have a smaller or larger residual error. When using the Moore-Penrose pseudo-inverse method to solve the system where the number of equations exceeds by far the number of parameters, the sum of the squared residues is brought to the minimum. Therefore, said approach can be used to obtain a simple-to-use and sufficiently precise functional approximation of the air-gap field.

Notice in (9) and (10) that the number of spatial harmonics taken into account is rather arbitrary, and it should be based on the previous experience. It is of interest to increase the number of harmonics in the analytical expressions, yet, on the other hand, this increases the number of coefficients, increases the calculation complexity, gives the rise to the numerical errors cause by the finite wordlength and it also makes the practical use of the final outcome more involved when it comes to designing and optimizing integrated charger topologies. In order to get an insight into the impact of the number of spatial harmonics on the consequential errors, the process is repeated several time with the top harmonic being the 11th, 13th, 15th, 17th and 19th. The evaluation is performed in following steps: (i) First, the MMF values are calculated in 20 time x 36 space = 720 individual points, (ii) After assembly of 720 equations, the relevant parameters are calculated by means of pseudo-inversion, (iii) The values of MMF are calculated from the functional approximation; (iv) In each point, the residual errors are obtained as the difference between the actual and approximation values, and these are used in (12); (v) The error ΔF is obtained as $\Sigma\Delta^2/\sum MMF_{WF}^2$, as illustrated in (12).

$$\Delta F_A = \sqrt{\frac{\sum_{i=1}^{20}\sum_{j=1}^{36}\left[MMF_{WF}(i,j)-MMF_{FA}(i,j)\right]^2}{\sum_{i=1}^{20}\sum_{j=1}^{36}\left[MMF_{WF}(i,j)\right]^2}} \tag{12}$$

Table 1 Residual errors (12) obtained after deriving the relevant parameters by Moore-Penrose pseudo-inversion

	19^{th}	17^{th}	15^{th}	13^{th}	11^{th}
6	$8.53\cdot10^{-13}$	$9.52\cdot10^{-13}$	15.62	15.62	15.62
9	$7.41\cdot10^{-13}$	$7.41\cdot10^{-13}$	$7.41\cdot10^{-13}$	6.78	6.78

The results are shown in Table 1, and they display the error (12) obtained for 6-phase and 9-phase topology, in cases where the highest order harmonics sweep from 11th up to the 19th. Notice in Table 1 that the error (12) is relative; the value of 1 corresponds to the case where the *rms* value of the error corresponds to the actual field. Therefore, the values that

exceed 1 are the indicators that the attempted functional approximation is fundamentally wrong.

In the case of a 6-phase machine, the error maintains considerable value until the 17th harmonic is taken into account. This circumstance is attributed to the existence of significant 17th harmonic which contributes to considerable errors when not taken into account. Further addition of the 19th harmonic into the approximation formula does not have any significant impact. In the case of a 9-phase machine, the error (12) remains high until the 15th harmonic is included into the functional approximation. This points out to the fact that the 15th harmonic of the air-gap field has considerable 15th harmonic, while the contribution of the 17th and 19th harmonics are negligible.

It is reasonable to assume that the computation complexity that is required to take into account the space-time harmonics in excess of the 19th is feasible. With a reasonable number of the slots within the stator magnetic circuit (which are expected to remain far below 100), the proposed 4-step process remains unharmed by the finite-wordlength errors and other issues related to calculation with very large matrices.

Thus, the 4-step process outlined and demonstrated in this Section provides the design tool for distinguishing and grading the stator winding configurations and the power converter topologies of integrated chargers. Some very important key features of the system can be envisaged from the content of pulsating and revolving air-gap field, made readily available by the proposed approach.

4. Applying the Proposed Method in Designing Integrated Chargers

Proposed approach is applied in evaluating the pulsating and revolving fields of four distinct designs, having different stator winding configurations and different number of phases in the static power converter. Considered are (i) The 6-phase integrated charger where the stator winding configuration is symmetrical, (ii) The 6-phase integrated charger where the stator winding configuration is asymmetrical, (iii) The 9-phase integrated charger where the stator winding configuration is symmetrical, (iv) The 9-phase integrated charger where the stator winding configuration is asymmetrical. In all the considered cases, the number of stator slots is equal to 36, and it is assumed that the winding has a single layer. The functional approximation includes all the relevant space-time harmonic, including the harmonic of the 19th order. The obtained results are summarized in Table 2 for both the charging mode and the traction mode.

With 6-phase asymmetrical machine running in charging mode, the relevant harmonics are the 5^{th}, 7^{th}, 17^{th} and 19^{th}, and all of them produce revolving fields. As a consequence, the electromagnetic torque assumes a non-zero value that depends on the magnitude of relevant harmonics fields.

When considering the 6-phase symmetrical machine in charging mode, the harmonic content is more populated, and it includes all the odd high order space-harmonics up to the 19^{th}, excluding only the 3^{rd}, 9^{th} and 15^{th}. What is particularly harmful is the presence of considerable first harmonic, having a large and unacceptable contribution to the electromagnetic torque. In the considered case, the traction motor would need a mechanical brake while running in charging mode. The change of the magnetic field along the stator circumference is obtained with symmetrical 6-phase machine and plotted in Fig. 5.

Considerable harmonic content contributes to a great deal of losses caused by harmonic fields.

Then a 9-phase machine is used within the integrated charger running in charging mode, the distribution of the MMF along the circumference is given in Fig. 6 for four consecutive instants of time. Proposed functional approximation ends with the 19th harmonic, and based upon these assumptions, the outcome of Table 2 includes the 3rd and the 15th harmonic different from zero (DFZ). Yet, when considering the error (12), the resulting value is exceptionally large, clearly indicating that there is a need to include more spatial harmonics.

Following a more thorough examinations, the findings are that the corresponding torque components caused by the charging currents in the 9-phase machine is used within the integrated charger are very small due to rather low values of revolving fields.

The results obtained with the 9-phase machine with asymmetrical stator windings used in charging mode are shown in Table 2, and they comprise the 3^{rd}, 9^{th} and the 15^{th} harmonic with a relatively low amplitude. Most of the components produce pulsating fields, and the revolving field content is negligible when compared to the revolving field of the first harmonic in the traction mode. Thus, the average value of the electromagnetic torque obtained in charging mode is negligible, as well as the relevant torque pulsations.

In the second part of the Table 2, the results correspond to the traction mode of all the considered configurations. The torque-generating currents have to be defined in the way prescribed by (1), excluding the intermediate phase transpositions and re-connections. With asymmetrical 6-phase machine, the field comprises only the 1^{st}, 5^{th} and 13^{th} harmonic, wherein the values of the 5^{th} and the 13^{th} harmonic are very small when compared to the fundamental. In symmetrical 6-phase machine, the fundamental component is accompanied by all the odd harmonic except for the 3rd, 9th and the 15th harmonic. The torque generation of 9-phase machines with asymmetrical and symmetrical stator winding is based on the approach given in [22], [25] and [26]. In addition to fundamental component, both symmetrical and asymmetrical 9-phase machines produce only the 17^{th} and 19^{th} harmonics, their values being considerably smaller than the fundamental.

The previous analysis, results and discussion outlines the application of the proposed 4-step approach in predicting the charging-mode and the traction-mode performances of the integrated charger with multiphase machines. The system losses and electromagnetic torque are estimated from the amplitudes of the pulsating and the revolving fields produced in the air-gap of multi-phase electrical machines. Out of the considered 4 design samples, the best results are obtained with the nine-phase setup employing asymmetrical stator winding.

The practical use of the proposed design tool stems from its ability to obtain a quick and precise estimate of the impact of several design parameters and features on the system performances in traction and charging modes. Considered design parameters include the number of phases of the electrical motor, the number of branches in static power converter, the number of layers and the implementation details of the stator winding, the winding connections and transpositions as well as selection of either symmetrical or asymmetrical winding dispositions. Drawback of the proposed algorithm is the need to repeat the pseudo-inverse-based parameter setting of the target functional approximation for each configuration and for each operating regime. In spite of that, related complexity and efforts are considerably reduced when compared to the approach which relies on FEM tools in each of the design phases.

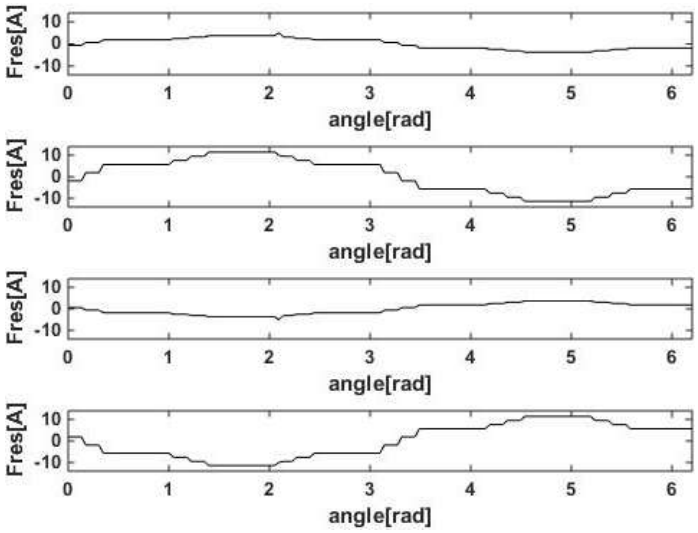

Fig. 5 The resultant MMF within the symmetrical 6-phase machine inside the charger described in [25]

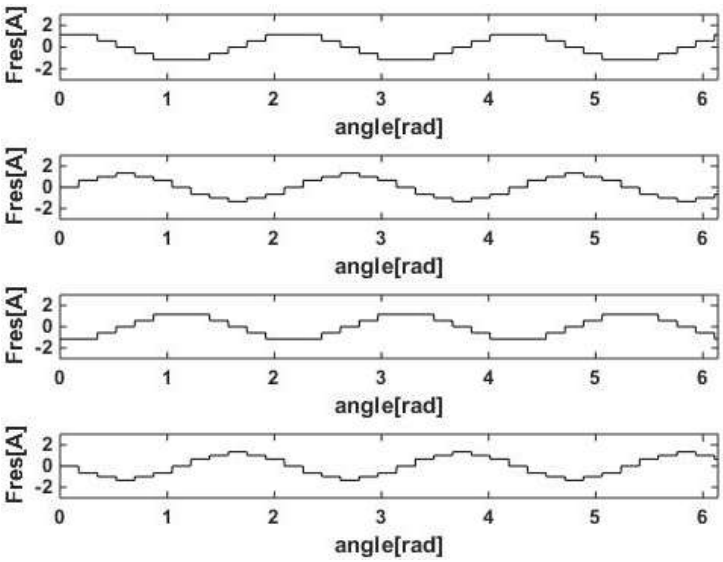

Fig. 6 The resultant MMF within the symmetrical nine-phase machine inside the charger described in [26]

Comparison of the proposed algorithm to other solutions that make use of [24] was not feasible. Vast majority of design approaches [19-22, 25-26] relies on some basic

analytical considerations and FEM tools. Compared to evidence given in [21], [22], [25], [26], as well as in references listed in review [20], the results of Figs. 3-6 and those of Table 2 provide valid conclusions and credible design guidelines.

Table 2 The harmonic content of magnetomotive force obtained from the stator winding with 36 slots and with scaled 1 Ampere-conductor located in each slot. Results are obtained for both charging and traction modes. The pulsating and revolving fields are resolved in the text which refers to this Table

Mode	Type	ν=1	ν=3	ν=5	ν=7	ν=11	ν=13	ν=15	ν=17	ν=19
Charge	6-asym	0	0	1.80	0.97	0	0	0	0.16	0.162
	6-sym	5.67	0	0.90	0.48	.06	0.05	0	0.08	0.081
	9-asym	0	0.41	0	0	0	0	0.03	0	0
	9-sym	0	DFZ	0	0	0	0	DFZ	0	0
Traction	6-asym	11.35	0	0.12	0	0	0.10	0	0	0
	6-sym	11.35	0	1.803	0.97	.12	0.10	0	0.16	0.0162
	9-asym	11.43	0	0	0	0	0	0	0.04	0.044
	9-sym	11.43	0	0	0	0	0	0	0.04	0.044

Results presented in this Section are not supported by the experimental evidence. Therefore, with the adopted assumptions and approximations, presented results could be better than in practical application. Experimental comparison of considerable number of machine-converter configurations was not feasible at this point. At the same time, the analysis and the design of the proposed procedures provide sufficient ground for the claim that the machine-configuration with superior predicted performances would outperform the others in practical application as well. Therefore, notwithstanding the absence of the experimental evidence, the proposed design method is capable of deriving the best machine-converter pair for the desired integrated charger.

5. CONCLUSIONS

The paper focuses on studying the air-gap field in multi-phase induction machines that are used in electrical vehicles with integrated chargers. It is found that the configuration of the stator windings as well as the topology of the integrated power converter largely affect the distribution of the air-gap field in both charging and traction modes, determining in this way the amplitudes of the revolving and pulsating magnetic fields. Said fields are proven to have the key impact on the losses, efficiency, pulsating torques and the torque-per-Amps ratio of the integrated traction-charger system. Based upon the analysis, a novel algorithm is proposed which determines the space-time distribution of the air-gap field, eventually deriving all the relevant performances, thus providing a practical and useful design tool. Proposed approach is tested on four characteristic design examples, and it proved efficient in studying the impact of the converter topology, number of phases and the configuration of the stator winding, providing at the same time the indications for further improvements of integrated battery chargers.

REFERENCES

[1] G. Kalghatgi, "Fuel/Engine Interactions", ISBN: 9780768080438, SAE, 2014.

[2] J. G. Zivin, M. Kotchen and E. Mansur, *Spatial and temporal heterogeneity of marginal emissions: Implications for electric cars and other electricity-shifting policies*. J. Econ. *Behavior & Org.* 2014, 107, 248–268.

[3] A. Elgowainy, J. Han, M. Mahalik, L. Poch, A. Rousseau, A. Vyas and M. Wang, *Well-to-Wheels Analysis of Energy Use and Greenhouse Gas Emissions of Plug-In Hybrid Electric Vehicles*. Argonne National Laboratory: Argonne IL, 2010.

[4] S. Haghbin, K. Khan, S. Lundmark, M. Alak¨ula, O. Carlson, M. Leksell, and O. Wallmark, "Integrated chargers for EV's and PHEV's: Examples and new solutions", In Proceedings of the 19th International Conference on Electrical Machines. Rome, 2010, pp. 1–6.

[5] L. Solero, "Nonconventional on-board charger for electric vehicle propulsion batteries*", IEEE Trans. Veh. Technol*., vol. 50, no. 1, pp. 144–149, Jan. 2001.

[6] M. Grenier, M. H. Aghdam and T. Thiringer, "Design of on-board charger for plug-in hybrid electric vehicle", In Proceedings of the International Conference on Power Electronics, Machine and Drives, 2010, pp. 1–6.

[7] M. Yilmaz, P.T. Krein, "Review of battery charger topologies, charging power levels, and infrastructure for plug-in electric and hybrid vehicles", *IEEE Trans. Power Electron*., vol. 28, no. 5, pp. 2151–2169, 2013.

[8] W. E. Rippel, "Integrated traction inverter and battery charger apparatus", U.S. Patent 4 920 475, Apr. 1990.

[9] G. Pellegrino, E. Armando and P. Guglielmi, "An integral battery charger with power factor correction for electric scooter", *IEEE Trans. Power Electron*., vol. 25, no. 3, pp. 751–759, Mar. 2010.

[10] F. Lacressonniere and B. Cassoret, "Converter used as a battery charger and a motor speed controller in an industrial truck", In Proceedings of the EPE, 2005, pp. 1–7.

[11] S. Haghbin, S. Lundmark and M. Alakula, "Grid-connected integrated battery chargers in vehicle applications: review and new solution", *IEEE Trans. Ind. Electron*., vol. 60, no. 2, pp. 459–473, 2013.

[12] M. Hinkkanen and J. Luomi, "Braking scheme for vector-controlled induction motor drives equipped with diode rectifier without braking resistor", In Proceedings of the 14th Industry Applications Conference. Kowloon, Hong Kong: 2005, vol. 2, pp. 1066–1072.

[13] A. G. Cocconi, "Combined motor drive and battery charger system", U.S. Patent 5 341 075, Aug. 1994.

[14] S. Lacroix, E. Laboure and M. Hilairet, "An integrated fast battery charger for electric vehicle", In Proceedings of the IEEE Vehicle and Power Propulsion Conference, Sep. 2010, pp. 1–6.

[15] S. Haghbin, S. Lundmark, M. Alakula, and O. Carlson, "An isolated high-power integrated charger in electrified vehicle applications", *IEEE Trans. Veh. Technol*., vol. 60, no. 9, pp. 4115–4126, Nov. 2011.

[16] J. K. Kamoun, N. B. Hadj, M. Chabchoub, R. Neji and M. Ghariani, "An induction motor FEM-based comparative study: Analysis of two topologies", In Proceedings of the 8th International Conference and Exhibition on Ecological Vehicles and Renewable Energies (EVER). Monte Carlo, 2013, pp. 1–5.

[17] Đ. Lekić and S. Vukosavić, "Finite Element Design of Rotor Permanent Magnet Flux Switching Machine with Arbitrary Slot, Pole and Phase Combinations", *Electronics*, vol. 22, no. 2, pp. 93–104, January 2019.

[18] S. Stipetić, W. Miebach and D. Žarko, "Optimization in Design of Electric Machines: Methodology and workflow", In Proceedings of the International ACEMP-OPTIMELECTROMOTION 2015 Joint Conference. Side, Turkey, 2-4 Sep. 2015, pp. 1–8.

[19] E. Levi, M. Jones, S. Vukosavic, et al., "A novel concept of a multiphase, multimotor vector controlled drive system supplied from a single voltage source inverter", *IEEE Trans. Power Electron*., vol. 19, no. 2, pp. 320–335, 2004.

[20] E. Levi, R. Bojoi, F. Profumo, F., et al., "Multiphase induction motor drives – a technology status review", *IET Electric Power Appl*., vol. 1, no. 4, pp. 489–516, 2007.

[21] I. Subotic, E. Levi, M. Jones, and D. Graovac, "An integrated battery charger for EVs based on an asymmetrical six-phase machine", In Proceedings of the IEEE Industrial Electronics Society Conference. Vienna, Austria, 2013, pp. 7242–7247.

[22] I. Subotic, N. Bodo, E. Levi, and M. Jones, "Onboard integrated battery charger for EVs using an asymmetrical nine-phase machine", *IEEE Trans. on Industrial Electronics*, vol. 62, no. 5, pp. 3285–3295, 2015.

[23] Penrose, Roger *(1955). A generalized inverse for matrices.* Proceedings of the Cambridge Philosophical Society, vol. 51, pp. 406–413.

[24] Penrose, Roger *(1956). On best approximation solution of linear matrix equations.* Proceedings of the Cambridge Philosophical Society, vol. 52, pp. 17–19.

[25] I. Subotic, E. Levi, M. Jones, and D. Graovac, "On-board integrated battery chargers for electric vehicles using nine-phase machines", In Proceedings of the IEEE International Electric Machines and Drives Conference. Chicago, IL, 2013, pp. 239–246.

[26] I. Subotic, N. Bodo, E. Levi, et al.: "Isolated chargers for EVs incorporating six-phase machines", *IEEE Trans. Ind. Electron*., vol. 63, no. 1, pp. 653-664, 2016.